HHS Public Access

Author manuscript

Cancer Res. Author manuscript; available in PMC 2023 March 02.

Published in final edited form as:

Cancer Res. 2022 September 02; 82(17): 3088–3101. doi:10.1158/0008-5472.CAN-22-0631.

CHD1 promotes sensitivity to Aurora kinase inhibitors by suppressing interaction of AURKA with its coactivator TPX2

Haoyan Li[1], **Yin Wang**[1], **Kevin Lin**[2], **Varadha Balaji Venkadakrishnan**[3], **Martin Bakht**[3], **Wei Shi**[1], **Chenling Meng**[1], **Jie Zhang**[1], **Kaitlyn Tremble**[1,4], **Xin Liang**[5], **Jian H. Song**[5], **Xu Feng**[1], **Vivien Van**[6], **Pingna Deng**[7], **Jared K. Burks**[8], **Ana Aparicio**[5], **Khandan Keyomarsi**[1], **Junjie Chen**[1], **Yue Lu**[2], **Himisha Beltran**[3], **Di Zhao**[1]

[1]Department of Experimental Radiation Oncology, The University of Texas MD Anderson Cancer Center, Houston, TX 77030, USA

[2]Department of Epigenetics and Molecular Carcinogenesis, The University of Texas MD Anderson Cancer Center, Houston, TX 77030, USA

[3]Division of Medical Oncology, Dana-Farber Cancer Institute, Boston, MA 02215, USA

[4]Honors College, Baylor University, Waco, TX 76706, USA

[5]Department of Genitourinary Medical Oncology, The University of Texas MD Anderson Cancer Center, Houston, TX 77030, USA

[6]Department of Imaging Physics, The University of Texas MD Anderson Cancer Center, Houston, TX 77030, USA

[7]Department of Cancer Biology, The University of Texas MD Anderson Cancer Center, Houston, TX 77030, USA

[8]Department of Leukemia, The University of Texas MD Anderson Cancer Center, Houston, TX 77030, USA

Abstract

Clinical studies have shown that subsets of cancer patients achieve a significant benefit from Aurora kinase inhibitors, suggesting an urgent need to identify biomarkers for predicting drug response. Chromodomain-helicase-DNA-binding protein 1 (CHD1) is involved in chromatin remodeling, DNA repair, and transcriptional plasticity. Prior studies have demonstrated that CHD1 has distinct expression patterns in cancers with different molecular features, but its impact on drug responsiveness remains understudied. Here, we show that CHD1 promotes the susceptibility of

Corresponding Author: Di Zhao, Department of Experimental Radiation Oncology, The University of Texas MD Anderson Cancer Center, 6565 MD Anderson Boulevard, Houston, Texas 77030, USA. Phone: 713-745-5214; dzhao2@mdanderson.org.

Authors' contributions

H.L. and D.Z. designed the research, analyzed the results, and wrote the manuscript. H.L. performed most of the experiments. D.Z. performed the GDSC pan-cancer association analyses. Y.W. provided mouse husbandry of GEMMs and assistance in animal experiments. Y.L., K.L., and M.B. performed the bioinformatics analysis for RNA-seq and the NEPC cancer database. V.B.V. performed the NEPC organoid culture and viability assays. W.S., C.M., J.S., X.F., and P.D. provided technical support. J.Z. helped with the preparation of pathological samples. X.L. provided pathological analysis. K.T. helped with the immunohistochemistry and cell viability assay. V.V. performed MRI scanning. J.K.B. helped with immunofluorescence imaging and data analysis. A.A., K.K., J.C., Y.L., and H.B. provided intellectual contributions throughout the project.

Conflicts of Interest: The authors have declared that no conflict of interest exists.

prostate cancer cells to inhibitors targeting Aurora kinases, while depletion of CHD1 impairs their efficacy in vitro and in vivo. Pan-cancer drug sensitivity analyses revealed that high expression of CHD1 was associated with increased sensitivity to Aurora kinase A (AURKA) inhibitors. Mechanistically, KPNA2 served as a direct target of CHD1 and suppressed the interaction of AURKA with the co-activator TPX2, thereby rendering cancer cells more vulnerable to AURKA inhibitors. Consistent with previous research reporting that loss of PTEN elevates CHD1 levels, studies in a genetically engineered mouse model, patient-derived organoids, and patient samples showed that PTEN defects are associated with a better response to AURKA inhibition in advanced prostate cancer. These observations demonstrate that CHD1 plays an important role in modulating Aurora kinases and drug sensitivities, providing new insights into biomarker-driven therapies targeting Aurora kinases for future clinical studies.

Introduction

Aurora kinases are key players in mitotic control. Three mammalian paralogues—Aurora A, B, and C—are very similar in amino acid sequence but have distinct subcellular localization and biological functions(1). During mitosis, Aurora A localizes to the centrosome and spindle microtubules and is required for centrosome maturation and mitotic spindle assembly(2–4). The activity of Aurora A can be modulated by autophosphorylation at Thr288(5,6), as well as by interaction with the co-activator TPX2(7,8). In the past decade, several small-molecule inhibitors targeting Aurora kinases have been tested in clinical trials. One such Aurora A inhibitor, alisertib, showed >200-fold higher selectivity for Aurora A than for Aurora B(9,10). Alisertib exhibited promising anti-tumor effects in numerous preclinical studies(11–13). Phase I and II trials showed that subsets of patients achieved significant clinical benefits from alisertib treatment, alone or in combination with other agents in lung, breast, and prostate cancers(14–17). Therefore, it is vital to identify the biomarkers for predicting response to alisertib and other Aurora kinase inhibitors.

Chromodomain helicase DNA binding protein 1 (CHD1) is involved in chromatin structure remodeling, nucleosome positioning, and gene transcriptional regulation, and thus plays important roles in multicellular organism development and embryonic stem cells pluripotency maintenance (18–21). Recurrent deletions of CHD1 occur in ~8% of prostate cancer patients (22,23). Loss of CHD1 causes DNA repair defects, androgen receptor redistribution and dysfunction, chromatin dysregulation, and transcriptional plasticity in prostate cancer(24–27). On the other hand, our prior studies(28,29) demonstrated that CHD1 is elevated in cancers containing PTEN defects, which occur in ~20% of primary and ~40% of castration-resistant prostate cancers (CRPC). How the distinct expression patterns of CHD1 affect the drug responsiveness in prostate cancers has not yet been determined.

Given the crucial role of CHD1 in epigenetic remodeling, here we performed an epigenetic screening in control and CHD1 knockout cells using 287 small-molecule inhibitors targeting 116 epigenetic factors. Interestingly, we found that CHD1 is involved in the susceptibility of tumor cells to Aurora A inhibitors. Then, we analyzed the correlation between CHD1 expression and the responses of cancer cells to Aurora kinase inhibitors in a pan-cancer drug sensitivity study. Furthermore, we demonstrated the role of CHD1 in promoting sensitivity

to Aurora A inhibitors both *in vitro* and *in vivo*, and elucidated the underlying mechanisms. Given that PTEN loss causes CHD1 elevation, we assessed the impact of PTEN defects on the efficacy of alisertib in preclinical models and explored the clinical relevance in patients with advanced prostate cancer.

Materials and Methods

Cell culture

All cell lines were obtained from ATCC, or Dr. Ronald A. DePinho's laboratory. All cell lines were cultured in medium supplemented with 10% FBS (Gibco, 10082147) and 1% penicillin/streptomycin (Gibco, 15140163) and incubated at 37 °C under 5% CO_2. DU145 cells were cultured in MEM medium (Corning, 10–010-CV). 293T, BPH1, PC-3M, and SK-LU-1 cells were cultured in DMEM medium (Corning, 10–017-CV). PC-3 cells were cultured in F-12K medium (ATCC, 30–2004). 22RV1, H211, LNCaP, A549, and H1299 cells were cultured in RPMI 1640 medium (Corning, 10–040-CV). All the cell lines were confirmed by UT MD Anderson's Cytogenetic and Cell Authentication Core, and were negative for mycoplasma using MycoAlert PLUS detection kit (Lonza, LT07–710) according to the manufacturer's instructions.

NEPC organoids culture

All NEPC organoids were cultured in advanced DMEM (Invitrogen) supplemented with 1× GlutaMAX (Invitrogen), 1% penicillin/streptomycin (Gibco), B27 (Gibco), 1.25 mM N-acetylcysteine (Sigma-Aldrich), 50 ng/ml mouse recombinant EGF (Invitrogen), 20 ng/ml human recombinant FGF-10 (Peprotech), 1 ng/ml recombinant human FGF-basic (Peprotech), 500 nM A-83–01 (Tocris), 10 μM SB202190 (Sigma-Aldrich), 10 mM nicotinamide (Sigma-Aldrich), 1 μM PGE2 (R&D Systems), 10 ng/ml NRG (VWR), Noggin-conditioned media (5%), and Rspondin-conditioned media (5%). All cell lines were confirmed to be mycoplasma-free and incubated at 37 °C under 5% CO_2.

Epigenetic screening

For the initial screening, 5×10^3 control or CHD1 KO BPH1 cells were seeded into 96-well plates (Corning, 3903) and treated with 287 compounds from Epigenetics Compound Library (Selleck, L1900) at 10μM for 72h. Cell viability was measured using CellTiter-Glo® Luminescent Cell Viability Assay Kit (Promega, G7573) according to the manufacturer's instructions. Cell viability in each well was normalized to DMSO control. The fold-change of cell viability in control versus CHD1 KO groups after each compound treatment was calculated individually and data was analyzed using excel and GraphPad Prism version 9.2.0 (RRID: SCR_002798). Twenty-four inhibitors targeting Aurora Kinase were selected for a second screening at two different doses. The original data of the initial and second screening were shown in Supplementary Table S1.

IC50 determination

Cancer cells were seeded into 96-well plates (Corning, 3903) and treated with DMSO or compounds at serial concentrations with three or four replicates for 72 h. NEPC organoids were seeded into 96-well plates (Corning, 3610) and treated with DMSO or alisertib at

serial concentrations with five replicates for 6 days. Cell viability was measured using the CellTiter-Glo Luminescent Cell Viability Assay kit (Promega, G7573) according to the manufacturer's instructions. Cell viability in each well was normalized and IC_{50} values were calculated using GraphPad Prism version 9.2.0.

Pan-cancer analyses of CHD1 expression and drug sensitivity

High-throughput drug screen data of 367 compounds in 987 human cancer cell lines were downloaded from the Genomics of Drug Sensitivity in Cancer (GDSC) database (https://www.cancerrxgene.org)(30,31). CHD1 mRNA expression data in 922 cancer cell lines were downloaded from the Cancer Cell Line Encyclopedia (CCLE) database(32). The Pearson correlation between CHD1 mRNA (z-score) and LN(IC_{50}) of individual compounds was analyzed (Supplementary Table S2). The Pearson correlation coefficient (r) and p values of all 367 compounds were calculated, and a volcano plot including the 367 compounds was generated using GraphPad Prism version 9.2.0. The correlations of CHD1 expression and IC_{50} of alisertib were analyzed and illustrated using GraphPad Prism version 9.2.0. Urogenital system cancer cell lines include cell lines of bladder, prostate, kidney, and endometrium cancers. Linear regression was calculated with 95% confidence bands of the best-fit line using GraphPad Prism version 9.2.0.

Apoptosis analyses

Cells were treated with control or 1 μM alisertib for 48 h. Then cells were collected and stained with FITC-annexin V (Invitrogen, A13199) and propidium iodide (Invitrogen, P1304MP) at room temperature for 15 min. Cell staining was detected using the Accuri C6 Flow Cytometer. All flow data were analyzed with FlowJo 10.6.1 (RRID: SCR_008520).

Transient transfection and Lentiviral transduction

Transient transfection of siRNA or plasmids was performed using Lipofectamine 2000 Transfection Reagent (Thermo Fisher Scientific, 11668019) according to the manufacturer's instructions. After 48 h, cells were used for further analyses. For lentiviral transduction, the lentiviral constructs, psPAX2 and pMD2.G were transfected into 293T cells using Lipofectamine 2000. After 48 h, viral supernatants were harvested and filtered. Transduced cells were incubated with viral supernatants and selected using puromycin (Gibco, A1113803) or Blasticidin S HCl (Gibco, A1113902). The information of siRNA, lentiviral constructs, and plasmids were shown in Supplementary Table S3.

Generation of CHD1 knockout cell lines using CRISPR

Plasmid pX330-Cherry-sg*CHD1* was transfected into BPH1, DU145, LNCaP, and 22Rv1 cells using Lipofectamine 2000 Transfection Reagent. After 72 h, 10 red fluorescent protein–positive cells were sorted into each well of a 96-well plate by flow cytometry. Single-cell colonies were chosen, followed by Western blot analysis of CHD1. The information of sgRNA were shown in Supplementary Table S3.

Quantitative PCR (qPCR)

Total RNA was extracted using RNeasy Mini Kit (Qiagen, 74104). cDNA was synthesized using the High-Capacity cDNA Reverse Transcription Kit (Applied Biosystems, 4368813) and used for qPCR reactions with PowerUp SYBR Green Master Mix (Applied Biosystems, A25779) by QuantStudio 3 Real-Time PCR Systems (Thermo Fisher Scientific). Gene-specific primers are listed in Supplementary Table S4. The relative mRNA levels of genes were normalized to that of ACTB. Each experiment was performed in triplicate. Data analysis was performed using GraphPad Prism version 9.2.0.

Chromatin immunoprecipitation (ChIP)-qPCR

BPH1 cells were fixed with 1% formaldehyde for 10 min, followed by quenching with glycine (2.5 M) for 5 min. Cells were washed with cold PBS and lysed with cell lysis buffer (12 mM Tris-HCl [pH 8.0], 10% PBS, 6 mM EDTA [pH 8.0], 12.5% FBS, 0.5% SDS, 1x Protease and Phosphatase Inhibitor (Thermo Scientific, 78442)) on ice for 15 min, followed by sonication using Bioruptor Pico (Diagenode). DNA fragment was immunoprecipitated with IgG or CHD1 antibody (Bethyl Laboratories, A301–218A, RRID: AB_890568) at 4 °C overnight. Target-bound DNA fragments were de-crosslinked and purified with phenol:chloroform:isoamyl alcohol (Invitrogen, 15593031) and chloroform:isoamyl alcohol (Sigma-Aldrich, C0549). The concentration of DNA was measured using a Qubit 4 Fluorometer (Invitrogen, Q33226) and Qubit™ 1X dsDNA High Sensitivity Assay Kit (Invitrogen, Q33230) according to the manufacturer's instructions. DNA was analyzed by qPCR using the KPNA2 promoter primers (Supplementary Table S4). The means and standard deviations of the normalized triplicate values were plotted using GraphPad Prism version 9.2.0.

RNA-sequencing and data analysis

Control and CHD1-knockout BPH1 cells were treated with DMSO or alisertib (10 μM) for 24 h. Then cells were lysed with TRIzol (Invitrogen, 15596026), and total RNA was extracted using RNeasy Mini Kit (Qiagen, 74104). The experiment was performed in triplicate. RNA sequencing was performed by MD Anderson Science Park Next Generation Sequencing Core, with 30–37 million pairs of reads per sample. The reads were mapped to the human genome hg38 using TopHat (version 2.0.10) (RRID: SCR_013035) (33). By reads, the overall mapping rate is 96%−97%; 94%−95% fragments have both ends mapped to the human genome. The number of fragments in each known gene from GENCODE Release 35(34) was enumerated using htseq-count from the HTSeq package (version 0.6.0) (RRID: SCR_005514)(35) (Supplementary Table S5). Genes with less than 10 fragments in all of the samples were removed before the differential expression analysis. The differential expression between conditions was statistically assessed using the R/Bioconductor package DESeq (version 1.18.0) (RRID: SCR_000154) (36). Genes with FDR (false discovery rate) ≤ 0.05, FC (fold change) ≥ 2, and length > 200 bp were called as differentially expressed. 618 differentially expressed genes (DEGs) that were elevated in alisertib-treated control or CHD1 KO cells (FDR≤0.05 and FC≥2) were used for heatmap generation. Hierarchical clustering was performed using Pearson distance method. Gene ontology analysis (https://

david.ncifcrf.gov) was performed using 439 DEGs that were uniquely elevated in control cells upon alisertib treatment but less changed in CHD1 KO cells.

Western blot analysis

Cells were lysed in 1x Laemmli Sample Buffer (Bio-Rad Laboratories, 1610747). Proteins were separated with 4%−15% Mini-PROTEAN TGX Precast Protein Gels (Bio-Rad, 4561086) and transferred to nitrocellulose membrane using Trans-Blot Turbo RTA Mini 0.2 μm Nitrocellulose Transfer Kit (Bio-Rad, 1704270), and incubated with anti-Aurora A (Cell Signaling Technology, 14475S, RRID: AB_2665504), anti-TPX2 (Cell Signaling Technology, 8559, RRID: AB_10827636), anti–Aurora B/AIM1 (Cell Signaling Technology, 3094S, RRID: AB_10695307), anti-CHD1 (D8C2) (Cell Signaling Technology, 4351S, RRID: AB_11179073), anti-KPNA2 (Cell Signaling Technology, 14372S, RRID: AB_2798467), anti-β-actin (8H10D10) (Cell Signaling Technology, 3700S, RRID: AB_2242334), anti–phospho-Aurora A (Thr288)/Aurora B (Thr232)/Aurora C (Thr198) (D13A11) (Cell Signaling Technology, 2914S, RRID: AB_2061631), anti–phospho-histone H3 (Ser10) (D2C8) (Cell Signaling Technology, 3377T, RRID: AB_1549592), anti-DYKDDDDK Tag (D6W5B) (Cell Signaling Technology, 14793, RRID: AB_2572291), anti-histone H3 (GenScript, A01502, RRID: AB_1968828), anti-PTEN (Cell Signaling Technology, 9188S, RRID: AB_2253290), anti-AKT (Cell Signaling Technology, 4691S, RRID: AB_915783), and anti-phospho-AKT (Ser473) (Cell Signaling Technology, 4060S, RRID: AB_2315049). Then the membrane was incubated with secondary antibodies anti-rabbit IgG (HRP) (Cell Signaling Technology, 7074V, RRID:AB_2099233), anti-mouse IgG (HRP) (Cell Signaling Technology, 7076V, RRID: AB_330924), and anti-rabbit IgG, light chain-specific (Jackson ImmunoResearch, 211-032-171, RRID: AB_2339149), followed by developing with Western ECL Substrates (Bio-Rad, 1705060, 1705062) and imaging by the ChemiDoc Imaging System (Bio-Rad).

Immunoprecipitation

The cell lysates were prepared in lysis buffer (20 mM Tris-HCl [pH 8.0], 0.4 M NaCl, 1 mM EDTA, 0.3% Nonidet P-40, and 1x Protease and Phosphatase Inhibitor) and incubated with anti-Aurora A (Cell Signaling Technology, 14475S, RRID: AB_2665504), or anti-TPX2 [18D5-1] (Abcam, ab32795, RRID: AB_778561), or normal mouse IgG (Millipore Sigma, 12–371, RRID: AB_145840), or normal rabbit IgG (Millipore Sigma, 12–370, RRID: AB_145841) overnight at 4 °C. Then Dynabeads Protein G (Thermo Fisher Scientific, 10009D) was added into the lysates, followed by incubation for an additional 4 h at 4 °C. For immunoprecipitation of Flag-tagged proteins, cell lysates were incubated with Anti-FLAG M2 Magnetic Beads (Millipore Sigma, M8823, RRID: AB_2637089) overnight at 4 °C. Then beads were washed with wash buffer (20 mM Tris-HCl [pH 8.0], 0.4 M NaCl, 1 mM EDTA, 0.1% Nonidet P-40, and 1x Protease and Phosphatase Inhibitor) and resuspended with 1x Laemmli Sample Buffer, followed by Western blot.

Dual luciferase reporter assay

The *KPNA2*-promoter region with putative CHD1-binding sites (~1.2 kb) (Supplementary table S3) was cloned into the pGL4 plasmid by Genewiz and verified by sequencing. LNCaP cells were transfected with vector control or the constructed pGL4 with *KPNA2* promoter,

Renilla control plasmid, and siControl or si*CHD1* using Lipofectamine 2000. After 72 h, cells were analyzed using the Dual-Luciferase Reporter Assay System (Promega, E1910) according to the manufacturer's instructions. Firefly and Renilla luciferase activity were read by the Synergy 2 Multi-Mode Microplate reader (BioTek). Firefly luciferase activity was normalized to the Renilla luciferase activity. Experiments were performed in triplicate, and statistical analyses were performed using GraphPad Prism version 9.2.0.

Site-directed mutagenesis

Precision LentiORF AURKA plasmid was used to generate Flag-tagged AURKA WT and S155R mutation expression plasmids using the Q5 Site-Directed Mutagenesis Kit (New England BioLabs, E0554S) according to the manufacturer's instructions. Plasmids were prepared using the QIAprep Spin Miniprep Kit (Qiagen, 27106) and sequenced by Genewiz. Mutagenesis primers (Supplementary Table S4) were designed by the NEBaseChanger website (http://nebasechanger.neb.com/).

In vivo Alisertib treatment

All mice were interbred and maintained at MD Anderson Cancer Center (Houston, TX), monitored for signs of ill health every day, and sacrificed and necropsied when moribund. All manipulations were performed under the review and approval of MD Anderson Cancer Center's Institutional Animal Care and Use Committee (Protocol #00001955). For establishing the xenograft model, male nude mice (6–8 weeks old) were purchased from the Experimental Radiation Oncology animal facility at MD Anderson and subcutaneously injected with control (2×10^6) or CHD1 knockout (3×10^6) DU145 cells into each flank. Once tumors reached approximately 100 mm^3, the mice were randomly assigned into two groups (n=6–8 per group) and treated with vehicle or alisertib (10 mg/kg/day, Selleck, S1133) by oral gavage daily. Tumor size was measured twice a week using calipers. Tumor volume was calculated (width × width × length/2). After a 21-day treatment, tumors were collected for histopathologic analyses.

Genetically engineered mouse model (GEMM) of *PB-Cre; Pten$^{L/L}$; Smad4$^{L/L}$ (PbPS)* were established as described previously(29) and were genotyped regularly. Tumor formation of *PbPS* mice was monitored by 7T-MRI. When tumor volume reached approximately 50 mm^3, tumor-bearing mice were randomly assigned into two groups (n=4–5 per group) and treated with vehicle or alisertib (20 mg/kg/day) by oral gavage daily. After a 25-day treatment, all mice were analyzed by 7T-MRI and sacrificed for tumor collection. The body weight of mice was monitored weekly.

Immunohistochemistry (IHC) and Immunofluorescence (IF)

Mouse tissues and organoids were paraffin embedded. H&E staining of mouse tissue was performed. The rehydrated sections were incubated in Antigen Unmasking Solution (Vector Laboratories, H-3300–250) at 95 °C for 30 min and 110 °C for 10 sec for antigen retrieval. For IHC, the sections were incubated with 0.3% H_2O_2 solution, supplemented with 50% methanol for 30 min to quench endogenous peroxidases, and then blocked with Rodent Block M (Biocare Medical, RBM961L) for 30 min. Primary antibodies were anti-Ki67 (Thermo Fisher Scientific, MA5-14520, RRID: AB_10979488), anti–cleaved

caspase-3 (Cell Signaling Technology, 9661S, RRID: AB_2341188), anti-phospho-H3 (Ser10) (Cell Signaling Technology, 3377T, RRID: AB_1549592), anti-phospho-Aurora A (Thr288)/Aurora B (Thr232)/Aurora C (Thr198) (D13A11) (Cell Signaling Technology, 2914, RRID:AB_2061631), anti-KPNA2 (Abcam, AB84440, RRID: AB_1860701), and anti-CHD1(Atlas Antibodies, HPA022236, RRID: AB_2670915). Rabbit-on-Rodent HRP-Polymer (Biocare Medical, RMR622L) was used for the secondary antibody interaction, and the DAB Quanto chromagen and substrate kit (Fisher Scientific, TA-125-QHDX) was used for development. The slides were scanned using an Aperio CS2 (Leica Biosystems). For IF, the rehydrated sections were blocked with blocking buffer (1× PBS, 3% donkey serum, 0.3% Triton X-100) for 60 min. Primary antibodies include anti-Aurora A (D3V7T) (Cell Signaling Technology, 91590S, RRID: AB_2800171), anti-TPX2 (18D5-1) (Abcam, ab32795, RRID: AB_778561), anti-KPNA2 (Abcam, AB84440, RRID: AB_1860701), and anti–alpha tubulin (YL1/2) (Invitrogen, MA1–80017, RRID: AB_2210201). Cross-Adsorbed secondary antibodies include Goat anti-Rat IgG, Alexa Fluor™ 647 (Invitrogen, A-21247, RRID: AB_141778), Goat anti-Mouse IgG, Alexa Fluor™ 594 (Invitrogen, A-11005, RRID: AB_141372), and Goat anti-Rabbit IgG, Alexa Fluor™ 488 (Invitrogen, A-11008, RRID: AB_143165). After DAPI staining (Thermo Fisher Scientific, P36941), sections were covered and scanned by the Vectra Polaris Imaging System (Akoya Biosciences). Quantification of p-Aurora or p-S10-H3 positive cells (10 individual views per group) was performed at 20× magnification using ImageJ (RRID: SCR_003070). Abnormal spindle assembly or TPX2-Aurora A co-localization (10 individual views per group) was quantified at 40× magnification using Phenochart 1.1.0. Statistical analyses were performed using GraphPad Prism version 9.2.0.

Clinical Relevance Analyses

Clinical cohorts(37,38) were mined to assess CHD1 expression across stages of prostate cancer progression (34 benign, 68 localized prostate cancer, 31 CRPC-Adeno, and 22 CRPC-NE). The results were expressed as the mean ± standard error of the mean (SEM). The differences between the two groups were compared using the unpaired Student's t-test. The statistical analysis was performed using Origin Pro 2020 (OriginLab Corporation, Northampton, MA, USA).

Expression of *CHD1*, *KPNA2*, *TPX2*, and *AURKA* genes and progression-free survival (DFS) data of 489 prostate cancer patients (TCGA) were downloaded from cbioportal (www.cbioportal.org). mRNA expression z-score relative to all samples (RNA Seq RPKM) was used to classify the "high (z-score>0)" and "low (z-score<0)" expression of each gene. Patients with CHD1 z-score>0 and KPNA2 z-score >0 were grouped as "$CHD1^{high}$/$KPNA2^{high}$", and patients with CHD1 z-score<0 and KPNA2 z-score <0 were grouped as "$CHD1^{low}$/$KPNA2^{low}$". The differences in DFS between the two groups were compared using Log-rank (Mantel-Cox) test. P-value and Hazard Ratio (log-rank) were calculated using GraphPad Prism version 9.2.0.. The same method was used for survival analysis of CHD1/TPX2 and CHD1/AURKA groups.

A Phase II trial of alisertib for patients with castration-resistant and neuroendocrine prostate cancer was published previously(17). Whole exome sequencing (WES) was performed in 48

tumor samples from 12 responders and 36 non-responders (17). PTEN defects were defined by homo- or hemi- deletions. The Pearson correlation of PTEN defects with response to alisertib was analyzed using GraphPad Prism version 9.2.0..

Data Availability Statement

The RNA-Seq datasets generated and analyzed during the current study are available in the GEO repository (GSE186633). The ChIP-Seq and ATAC-Seq data analyzed during this study were generated and published in this research article(29): *Chromatin Regulator, CHD1, Remodels Immunosuppressive Tumor Microenvironment in PTEN-Deficient Prostate Cancer. Cancer Discov. 2020 May 8; CD-19–1352. doi:* 10.1158/2159-8290.

Statistical Analyses

All data are presented as the mean ± standard deviation of at least triplicate experiments. Statistical analyses were performed using GraphPad Prism version 9.2.0. Pairwise comparisons were performed using an unpaired two-tailed Student *t*-test. ****p<0.0001, ***p<0.001, **p<0.01, *p<0.05.

Results

CHD1 renders cancer cells vulnerable to inhibitors targeting Aurora A.

To determine the impact of CHD1 on the sensitivity of cancer cells to epigenetic inhibitors, we performed epigenetic screening using a small-molecule inhibitor library containing 287 compounds targeting 116 epigenetic factors in control and CHD1 depleted prostatic hyperplasia cells (Fig. 1A–B and Supplementary Table S1). In the initial and secondary screens, we found that *CHD1* knockout reduced the efficacies of Aurora kinase inhibitors, especially the compounds that selectively or preferentially target Aurora A (Fig. 1B and Supplementary Fig. S1A and S1B). Next, we determined the impact of CHD1 on the susceptibility of diverse prostate cancer cell lines to Aurora A-selective inhibitors, alisertib and MK-5108. The results showed that CRISPR-Cas9-directed *CHD1* knockout caused a 3- to 15-fold increase in the IC_{50} values of Aurora A inhibitors in these cells (Fig. 1C–D and Supplementary Figs. S1C–S1D). PC-3M is a metastasis-derived variant of prostate cancer cell line PC-3. Compared to PC-3, PC-3M cells expressed a higher level of CHD1 and were more sensitive to alisertib and MK5108 (Fig. 1E, and Supplementary Fig. S1E), whereas depletion of CHD1 rendered PC-3M cells more resistant (Fig. 1F). These studies revealed that CHD1 contributes to the susceptibility of prostate cancer cells to Aurora A inhibitors.

To explore CHD1's impact on drug sensitivity at a pan-cancer level, we integrated the CHD1 expression profiles from CCLE and the drug susceptibility profiles of 367 compounds from the GDSC database (Supplementary Fig. S2A and Supplementary Table S2). Pearson correlation analyses in ~600 cancer cell lines showed that CHD1 high expression was associated with better responses to inhibitors targeting Aurora A, including alisertib (Fig. 1G; Supplementary Fig. S2B and S2C). In addition to urogenital system cancer cells, we also found positive correlations of CHD1 expression with alisertib sensitivity in cancer cells of the colon, liver, and lung (Fig. 1H and Supplementary Figs. S2D and S2E). Thus, we determined the dose-response of alisertib in lung cancer cell lines containing intact or

deficient *CHD1*. The results showed that CHD1-deficient cells were less sensitive to Aurora A inhibitors (Supplementary Fig. S2F). Knocking down *CHD1* using siRNA remarkably reduced the susceptibility of CHD1-intact cells to alisertib (Supplementary Fig. S2G); in contrast, CHD1 overexpression in CHD1-deficient cancer cells augmented their sensitivity to alisertib (Supplementary Fig. S2H).

Collectively, the epigenetic screening, pan-cancer drug sensitivity analyses, and functional validations in prostate and lung cancer cells demonstrated that CHD1 high expression renders cancer cells vulnerable to inhibitors targeting Aurora A, while *CHD1* deletion causes the resistance to those inhibitors. To be noted, we also determined the IC50 values of several non-Aurora A targeting agents, including inhibitors of VEGFR or KRAS pathway. As shown in Supplementary Fig. S2I, *CHD1* knockout has minimal effects on their efficacies, suggesting CHD1's impact on drug sensitivity is not a general effect. Therefore, it is crucial to understand the mechanism by which CHD1 specifically promotes the susceptibility of cancer cells to Aurora A inhibitors.

CHD1 is required for the apoptotic process induced by Aurora A inhibitor.

As alisertib has progressed to phase III clinical trials in various tumor types, we mainly used alisertib for mechanistic studies. Consistent with prior study(39), alisertib significantly reduced cell growth and induced early- and late-stage apoptosis in control cells; however, depletion of CHD1 partially impaired the anti-proliferation and pro-apoptosis effects of alisertib (Fig. 2A and Supplementary Fig. S2J).

To capture changes in the transcriptome landscape, we performed RNA sequencing in control and CHD1-depleted cells with or without alisertib treatment. The differential gene expression analysis showed that alisertib caused the upregulation of 528 genes and downregulation of 109 genes in control cells; in contrast, only 195 upregulated genes and 32 downregulated genes were found in CHD1-depleted cells (Fig. 2B, fold change ≥2; false discovery rate ≤0.05). Then, we performed hierarchical clustering analysis using 618 differentially expressed genes (DEGs) that were significantly elevated in alisertib-treated control or CHD1 knockout cells. Notably, 71% of DEGs (439/618) were transcriptionally activated by alisertib in control cells, but not in CHD1-depleted cells (Fig. 2C). Gene Ontology analysis revealed that those uniquely elevated genes were highly enriched in the apoptotic process (Fig. 2D). Altogether, these functional studies and transcriptional profiling suggested that CHD1 is involved in apoptosis induced by Aurora A inhibitors.

CHD1 controls Aurora A by modulating its interaction with TPX2.

To understand how CHD1 promotes alisertib sensitivity, we assessed the impact of CHD1 on Aurora A expression and phosphorylation. As shown in Figure 3A, CHD1 depletion has no effect on total Aurora A but increases its phosphorylation at Thr288. Alisertib treatment caused a reduction of Thr288 phosphorylation in control cells in a dose-dependent manner (Fig. 3B). In contrast, CHD1-depleted cells retained phosphorylation of Aurora A in the presence of alisertib (Fig. 3B). Microtubule-associated protein TPX2 serves as a co-activator of Aurora A(7,8). The binding of TPX2 prevents the dephosphorylation of Aurora A and enhances the kinase activity(5,7,40–43). But TPX2 displays a much weaker

binding affinity to Aurora B(44). The prior structural study revealed that TPX2 binding triggers a conformational change of Aurora A and retains the kinase in an active state, which is less sensitive to alisertib (45). Thus, we assessed the interaction of Aurora A with TPX2 in the presence or absence of CHD1. Co-immunoprecipitation assays revealed that depletion of CHD1 remarkably enhances the binding of TPX2 to Aurora A, but not Aurora B, particularly in the presence of alisertib (Fig. 3C; Supplementary Fig. S3A).

To determine whether TPX2 mediates the resistance of CHD1-deficient cells to Aurora A inhibitors, we knocked out *TPX2* in control and CHD1-depleted cells (Fig. 3D). The drug response studies showed that *TPX2* knockout markedly increased alisertib sensitivity of CHD1-depleted cells, but only had a moderate effect on control cells (Fig. 3 E). Next, we disrupted the interaction between Aurora A and TPX2 by replacing the endogenous Aurora A with a Flag-tagged S155R mutant(46) (Supplementary Fig. S3B). Co-immunoprecipitation assays confirmed that the S155R mutant successfully diminished the Aurora A-TPX2 interaction regardless of the presence of alisertib (Fig. 3F; Supplementary Fig. S3C). Phenocopying of *TPX2* knockout, the disruption of Aurora A-TPX2 interaction rendered CHD1-depleted cells more sensitive to Aurora A inhibitor (Fig. 3G). These results established the role of CHD1 in modulating Aurora kinase activation via restraining its binding to the co-activator TPX2. These studies provide mechanistic insights into the differential responses of CHD1-high and CHD1-low cancer cells to Aurora A-targeted drugs.

The axis of CHD1-KPNA2 controls the interaction of TPX2 and Aurora A.

Importin-α (KPNA) family proteins interact with and silence the activity of TPX2(47,48). When cells enter mitosis, a gradient of Ran-GTP near chromosomes releases TPX2 from importin-α and promotes the binding of TPX2 to Aurora A(49,50). Among seven KPNA family genes, we found that the expression of KPNA2 was most significantly downregulated upon *CHD1* deletion (Fig. 4A; Supplementary Figs. S4A and S4B). Conversely, overexpression of CHD1 elevated KPNA2 in prostate cancer cells (Supplementary Fig. S4C). Expression analysis in human prostate cancers also revealed a positive correlation between CHD1 and KPNA2 (Fig. 4B).

Given that CHD1 plays a key role in chromatin assembly and gene transcriptional regulation, ATAC sequencing was performed using control versus CHD1-depleted prostate cancer cells(29). The results showed that promoter accessibility of the *KPNA2* gene was decreased upon CHD1 depletion (Fig. 4C). ChIP-sequencing using a murine prostate cancer cell line(29), revealed that CHD1 protein bound to the promoter region of the *Kpna2* gene (Supplementary Fig. S4D). This observation was further validated in human prostate cancer cells by ChIP-qPCR (Supplementary Fig. S4E). Dual luciferase assays revealed that CHD1 contributes to the transcriptional activation of the *KPNA2* gene (Fig. 4D).

Furthermore, we determined the loss-of-function effects of KPNA2 in modulating Aurora kinase and the response to Aurora A inhibitor. In the presence of alisertib, knockout of *KPNA2* preserved the Aurora A-TPX2 interaction and Aurora kinase activity characterized by histone H3 phosphorylation (p-S10-H3) (Fig. 4E; Supplementary Figs. S4F and S4G). Phenocopying *CHD1* deletion, *KPNA2* knockout reduced the susceptibility of cancer cells

to alisertib and protected them from alisertib-induced apoptosis (Fig. 4F; Supplementary Fig S4H). Conversely, overexpression of KPNA2 increased the susceptibility of CHD1-low prostate cancer cells to alisertib (Supplementary Fig S4I). Together, these mechanistic studies demonstrated that the regulatory axis of CHD1-KPNA2 modulates TPX2-Aurora A interaction and thereby promotes sensitivity to Aurora A inhibitors.

CHD1 is required for the anti-tumor effects of alisertib *in vivo*.

Next, we assessed *in vivo* efficacy of alisertib in xenograft models derived from control and CHD1-depleted DU145 cells. As shown in Figure 5A, CHD1 depletion had minimal impact on tumor growth, but greatly impaired the anti-tumor efficacy of alisertib *in vivo*. Alisertib administration was well tolerated by mice (Supplementary Fig. S5A). Molecular biomarker staining indicated KPNA2 expression was remarkably downregulated in CHD1-depleted xenograft tumors (Fig. 5B). Besides, treatment with alisertib inhibited cancer cell proliferation and induced apoptosis in control tumors; however, it had much less effect on CHD1-depleted tumors (Fig. 5C). Consistent with our observations *in vitro*, CHD1-depleted tumors retained the phosphorylation and activity of Aurora kinases after alisertib treatment (Fig. 5C; Supplementary Figs. S5B and S5C). Furthermore, IF staining in xenograft tumors revealed that CHD1 depletion preserved the co-localization of TPX2 and Aurora A on mitotic spindles in the presence of alisertib (Fig. 5D). Given that TPX2-Aurora A interaction is required for spindle assembly during mitosis(8,51), we determined the chromosome alignment and mitotic spindle assembly. The results showed that alisertib treatment caused a high percentage of abnormal spindles in control xenograft tumors, but this effect was rescued by *CHD1* depletion (Fig. 5E; Supplementary Figs. S5D and S5E).

These studies in xenograft models provide *in vivo* evidence for the role of CHD1 in mediating the anti-tumor effects of Aurora A inhibitors in prostate cancer via regulating KPNA2 and TPX2-Aurora interaction. In prostate cancer patients, we found that *CHD1* mRNA expression is significantly elevated in CRPC (Fig. 5F), and high expression of CHD1 and KPNA2 was associated with worse Progression-Free Survival (PFS) (Fig. 5G). In addition, prostate cancer patients with high expression levels of CHD1/AURKA or CHD1/TPX2 also showed worse PFS (Fig. 5H and Supplementary Fig. S5F). These clinical relevance analyses implicate the therapeutic potential of Aurora A inhibitors in subsets of prostate cancers expressing high levels of CHD1 and other potent biomarkers.

PTEN defects are associated with a better response to alisertib.

Given the regulatory role of the PTEN-AKT pathway in CHD1 elevation in prostate cancer(28), here we determined the impact of PTEN and AKT on alisertib sensitivity. To this end, we knocked down *PTEN* using siRNA in DU145 cells and found activated AKT, elevated CHD1, and increased sensitivity to alisertib (Fig. 6A and Supplementary Fig. S6A). Conversely, inhibition of AKT with MK2206 led to a reduction of CHD1 protein and diminished the efficacy of alisertib in a dose-dependent manner (Supplementary Fig. S6B–S6C). Similar to CHD1, we found AKT1 expression positively correlated with alisertib sensitivity in urogenital system cancers (Supplementary Fig. S6D). These results indicated that the PTEN-AKT pathway, as the upstream regulator of CHD1, is involved in modulating sensitivity to Aurora A inhibitors.

Next, we tested the *in vivo* efficacy of alisertib in a PTEN-deficient GEMM, which contains prostate-specific co-deletion of *Pten* and *Smad4* genes *(so-called PbPS, PB-Cre; Pten$^{L/L}$; Smad4$^{L/L}$*). Our prior study showed that PbPS mice developed highly invasive prostate adenocarcinoma, which highly expressed CHD1(29,52). As shown in Fig. 6B–D and Supplementary Figs. S6E–S6F, alisertib treatment significantly suppressed tumor growth of PbPS mice and has no visible toxicity. Histopathologic analyses revealed that Aurora A inhibitor remarkably delayed the progression and invasion of PTEN-deficient prostate tumors (Fig. 6E; Supplementary Figs. S6G), suppressed cancer cell proliferation, and induced apoptosis *in vivo* (Fig. 6F).

At last, we determined the clinical relevance between PTEN defects and response to Aurora A inhibitor in clinical study of alisertib(17). Among 48 patients with castration-resistant and neuroendocrine prostate cancers, we found that PTEN defects were associated with a better response to alisertib (Fig. 6G). Two patient-derived NEPC organoid lines, PM154 and PM155, were developed from the pretreatment biopsies in this clinical study(17). Organoid line PM154 was derived from the tumor of a non-responder patient with intact PTEN, while PM155 was from an exceptional responder containing PTEN loss (17,53). Compared to PM154, PTEN-deficient PM155 organoids expressed higher levels of CHD1 and KPNA2 and were much more sensitive to alisertib (Fig. 6H–I). Together, these studies in preclinical mouse models and human samples suggested prostate cancers containing PTEN defects and high CHD1 expression are more sensitive to Aurora A inhibitors.

Discussion

Through epigenetic screening, pan-cancer drug sensitivity analyses, and functional validation *in vitro* and *in vivo*, here we established a novel role of CHD1 in promoting the susceptibility of cancer cells to Aurora A inhibitors. Mechanistically, we identified a new regulatory axis of CHD1-KPNA2-TPX2, which plays a key role in modulating Aurora A activation (Fig. 6J). PTEN-defects induced CHD1 elevation augments the transcription of *KPNA2* and thereby restrains the interaction of TPX2 to Aurora A. Without TPX2's binding, inhibitors can effectively suppress the activity of Aurora A, resulting in spindle assembly defects and apoptosis. In CHD1 deficient cells, the increased TPX2 binding preserves the kinase activity of Aurora A and renders cancer cells more resistant to Aurora A-targeted therapy (Fig. 6J).

To date, several small-molecule inhibitors targeting Aurora kinases have been tested in clinical trials in patients with advanced solid tumors and leukemia. Phase I and II trials showed that certain subsets of patients achieved greater clinical benefit than others(14–17,54). Our studies demonstrated that the axis of CHD1-KPNA2 governs the interaction between TPX2 and Aurora A and sensitizes cancer cells to inhibitors targeting Aurora kinases. Given that high expression of CHD1 and KPNA2 was associated with worse PFS in prostate cancer patients and was found in the patient-derived organoids from the exceptional responder to alisertib, they might be potential predictive biomarkers. Further study is needed to determine their expression patterns at both mRNA and protein levels in responders versus non-responders in clinical studies of Aurora kinase inhibitors.

Genetic deletion and mutations of the *PTEN* gene occur in ~40% of CRPC and are associated with metastatic disease and poor overall outcome (55,56). Our previous studies demonstrated that PTEN defects caused the upregulation of CHD1, which mediates prostate cancer progression via cell-intrinsic and -extrinsic mechanisms(28,29). Our current studies uncovered the vulnerability of CHD1 elevation in PTEN-deficient tumors, that is the increased sensitivity to Aurora A inhibitors. The link between the PTEN-CHD1 axis and the susceptibility to Aurora A inhibitors was further established by preclinical studies using human cell lines and mouse models, as well as the correlation analysis of *PTEN* gene status with responses to alisertib in patients with advanced prostate cancers. Given that *PTEN* genetic testing has been used for clinical management of prostate and other cancer types, our studies provide new insights for using PTEN as a predictive marker to improve the patient selections in clinical trials of alisertib and other Aurora A inhibitors.

Recent large-scale cancer genome studies identified the genetic deletion and mutations of *CHD1* in ~8% of prostate cancers and other cancer types. Prior studies found CHD1 loss enhanced responsiveness to DNA-damaging therapy, such as PARP inhibitors(24,25). Our studies demonstrated that CHD1 deficiency causes the resistance of prostate tumors to Aurora A inhibitors by augmenting the binding of TPX2 to Aurora A. It may explain the poor responsiveness in some patients in clinical studies. Several new strategies have been developed to target Aurora A, such as PROTAC-mediated degradation of Aurora A protein and impedance of the TPX2-Aurora A interaction(57,58). These approaches may be potent to reverse the resistance mechanism and achieve better therapeutic effects when combined with alisertib in cancers harboring CHD1 deficiency.

In addition to CHD1, we also found other CHD family members, such as CHD4 and CHD8, associated with alisertib sensitivity in the pan-cancer drug sensitivity analyses. However, CHD1 showed the most significant correlation with alisertib sensitivity in cancer cells of the urogenital system, lung, colon, and liver. Given that CHD family genes have similar chromatin remodeling activities, they may share similar functions when modulating Aurora kinases and drug sensitivity, but different members may play predominant roles in different contexts. The findings in this study will inform future studies of other CHD members in diverse cancer types. Besides CHD family, other proteins, such as SH2D3C, TNFRSF12A, SDC4, RHBDF1, and PPIC, showed even stronger associations with alisertib sensitivity in the pan-cancer analyses, therefore, it is worthy to further explore the underlying mechanisms and evaluate their potential as predictive biomarkers in cancers.

Supplementary Material

Refer to Web version on PubMed Central for supplementary material.

Acknowledgments

The authors thank Dr. Ronald A. DePinho (MD Anderson Cancer Center) for sharing A549, H1299, NCI-H211 and SK-LU-1 cells. The authors thank Ann Sutton and Sarah Bronson in the Editing Services of Research Medical Library at The University of Texas MD Anderson Cancer Center for editing the article. This research was performed in the MD Anderson Cancer Center Flow Cytometry and Cellular Imaging Core Facility, which is supported in part by the National Institutes of Health (NIH) through MD Anderson Cancer Center Support Grant CA016672 and the National Cancer Institute's Research Specialist 1 R50 CA243707-01A1. RNA sequencing

was performed by the MD Anderson Cancer Center Science Park Next-Generation Sequencing Core, supported by Cancer Prevention and Research Institute of Texas (CPRIT) Core Facility Support Award RP170002. We also acknowledge the MD Anderson Functional Genomics Core as well as the Small Animal Imaging Facility, which is supported by the NIH under award number P30CA016672. This study was supported by the Prostate Cancer Foundation Young Investigator Award 17YOUN18 (to D. Zhao), NIH Pathway to Independence Award-NCI R00CA226360 (to D. Zhao), and CPRIT Recruitment of First-Time Tenure-Track Faculty Award RR190021 (to D. Zhao, a CPRIT Scholar in Cancer Research).

Authors' Disclosures

D. Zhao reports grants from NCI and Prostate Cancer Foundation during the conduct of the study. No disclosures were reported by the other authors.

References

1. Carmena M, Earnshaw WC. The cellular geography of aurora kinases. Nat Rev Mol Cell Biol 2003;4(11):842–54 doi 10.1038/nrm1245. [PubMed: 14625535]
2. Hannak E, Kirkham M, Hyman AA, Oegema K. Aurora-A kinase is required for centrosome maturation in Caenorhabditis elegans. J Cell Biol 2001;155(7):1109–15 doi DOI 10.1083/jcb.200108051. [PubMed: 11748251]
3. Glover DM, Leibowitz MH, McLean DA, Parry H. Mutations in aurora prevent centrosome separation leading to the formation of monopolar spindles. Cell 1995;81(1):95–105 doi 10.1016/0092-8674(95)90374-7. [PubMed: 7720077]
4. Berdnik D, Knoblich JA. Drosophila aurora-A is required for centrosome maturation and actin-dependent asymmetric protein localization during mitosis. Curr Biol 2002;12(8):640–7 doi 10.1016/S0960-9822(02)00766-2. [PubMed: 11967150]
5. Littlepage LE, Wu H, Andresson T, Deanehan JK, Amundadottir LT, Ruderman JV. Identification of phosphorylated residues that affect the activity of the mitotic kinase Aurora-A. P Natl Acad Sci USA 2002;99(24):15440–5 doi 10.1073/pnas.202606599.
6. Walter AO, Seghezzi W, Korver W, Sheung J, Lees E. The mitotic serine/threonine kinase Aurora2/AIK is regulated by phosphorylation and degradation. Oncogene 2000;19(42):4906–16 doi DOI 10.1038/sj.onc.1203847. [PubMed: 11039908]
7. Bayliss R, Sardon T, Vernos I, Conti E. Structural basis of Aurora-A activation by TPX2 at the mitotic spindle. Mol Cell 2003;12(4):851–62 doi Doi 10.1016/S1097-2765(03)00392-7. [PubMed: 14580337]
8. Kufer TA, Sillje HHW, Koerner R, Gruss OJ, Meraldi P, Nigg EA. Human TPX2 is required for targeting Aurora-A kinase to the spindle. Cell Motil Cytoskel 2003;54(2):179-.
9. Manfredi MG, Ecsedy JA, Chakravarty A, Silverman L, Zhang M, Hoar KM, et al. Characterization of Alisertib (MLN8237), an investigational small-molecule inhibitor of aurora A kinase using novel in vivo pharmacodynamic assays. Clin Cancer Res 2011;17(24):7614–24 doi 10.1158/1078-0432.CCR-11-1536. [PubMed: 22016509]
10. Gorgun G, Calabrese E, Hideshima T, Ecsedy J, Perrone G, Mani M, et al. A novel Aurora-A kinase inhibitor MLN8237 induces cytotoxicity and cell-cycle arrest in multiple myeloma. Blood 2010;115(25):5202–13 doi 10.1182/blood-2009-12-259523. [PubMed: 20382844]
11. Mehra R, Serebriiskii IG, Burtness B, Astsaturov I, Golemis EA. Aurora kinases in head and neck cancer. Lancet Oncol 2013;14(10):E425–E35 doi Doi 10.1016/S1470-2045(13)70128-1. [PubMed: 23993387]
12. Pitts TM, Bradshaw-Pierce EL, Bagby SM, Hyatt SL, Selby HM, Spreafico A, et al. Antitumor activity of the aurora a selective kinase inhibitor, alisertib, against preclinical models of colorectal cancer. Oncotarget 2016;7(31):50290–301 doi 10.18632/oncotarget.10366. [PubMed: 27385211]
13. Brockmann M, Poon E, Berry T, Carstensen A, Deubzer HE, Rycak L, et al. Small molecule inhibitors of aurora-a induce proteasomal degradation of N-myc in childhood neuroblastoma. Cancer Cell 2013;24(1):75–89 doi 10.1016/j.ccr.2013.05.005. [PubMed: 23792191]
14. Falchook G, Coleman RL, Roszak A, Behbakht K, Matulonis U, Ray-Coquard I, et al. Alisertib in Combination With Weekly Paclitaxel in Patients With Advanced Breast Cancer or Recurrent

Ovarian Cancer: A Randomized Clinical Trial. JAMA Oncol 2019;5(1):e183773 doi 10.1001/jamaoncol.2018.3773. [PubMed: 30347019]

15. Melichar B, Adenis A, Lockhart AC, Bennouna J, Dees EC, Kayaleh O, et al. Safety and activity of alisertib, an investigational aurora kinase A inhibitor, in patients with breast cancer, small-cell lung cancer, non-small-cell lung cancer, head and neck squamous-cell carcinoma, and gastro-oesophageal adenocarcinoma: a five-arm phase 2 study. Lancet Oncol 2015;16(4):395–405 doi 10.1016/S1470-2045(15)70051-3. [PubMed: 25728526]
16. DuBois SG, Mosse YP, Fox E, Kudgus RA, Reid JM, McGovern R, et al. Phase II Trial of Alisertib in Combination with Irinotecan and Temozolomide for Patients with Relapsed or Refractory Neuroblastoma. Clin Cancer Res 2018;24(24):6142–9 doi 10.1158/1078-0432.CCR-18-1381. [PubMed: 30093449]
17. Beltran H, Oromendia C, Danila DC, Montgomery B, Hoimes C, Szmulewitz RZ, et al. A Phase II Trial of the Aurora Kinase A Inhibitor Alisertib for Patients with Castration-resistant and Neuroendocrine Prostate Cancer: Efficacy and Biomarkers. Clin Cancer Res 2019;25(1):43–51 doi 10.1158/1078-0432.CCR-18-1912. [PubMed: 30232224]
18. Gaspar-Maia A, Alajem A, Polesso F, Sridharan R, Mason MJ, Heidersbach A, et al. Chd1 regulates open chromatin and pluripotency of embryonic stem cells. Nature 2009;460(7257):863–8 doi 10.1038/nature08212. [PubMed: 19587682]
19. Baumgart SJ, Najafova Z, Hossan T, Xie W, Nagarajan S, Kari V, et al. CHD1 regulates cell fate determination by activation of differentiation-induced genes. Nucleic Acids Res 2017;45(13):7722–35 doi 10.1093/nar/gkx377. [PubMed: 28475736]
20. Farnung L, Vos SM, Wigge C, Cramer P. Nucleosome-Chd1 structure and implications for chromatin remodelling. Nature 2017;550(7677):539–42 doi 10.1038/nature24046. [PubMed: 29019976]
21. Tsukiyama T The in vivo functions of ATP-dependent chromatin-remodelling factors. Nat Rev Mol Cell Biol 2002;3(6):422–9 doi 10.1038/nrm828. [PubMed: 12042764]
22. Hoadley KA, Yau C, Hinoue T, Wolf DM, Lazar AJ, Drill E, et al. Cell-of-Origin Patterns Dominate the Molecular Classification of 10,000 Tumors from 33 Types of Cancer. Cell 2018;173(2):291–304 e6 doi 10.1016/j.cell.2018.03.022. [PubMed: 29625048]
23. Burkhardt L, Fuchs S, Krohn A, Masser S, Mader M, Kluth M, et al. CHD1 Is a 5q21 Tumor Suppressor Required for ERG Rearrangement in Prostate Cancer. Cancer Res 2013;73(9):2795–805 doi 10.1158/0008-5472.Can-12-1342. [PubMed: 23492366]
24. Shenoy TR, Boysen G, Wang MY, Xu QZ, Guo W, Koh FM, et al. CHD1 loss sensitizes prostate cancer to DNA damaging therapy by promoting error-prone double-strand break repair. Ann Oncol 2017;28(7):1495–507 doi 10.1093/annonc/mdx165. [PubMed: 28383660]
25. Kari V, Mansour WY, Raul SK, Baumgart SJ, Mund A, Grade M, et al. Loss of CHD1 causes DNA repair defects and enhances prostate cancer therapeutic responsiveness. EMBO Rep 2018;19(10) doi 10.15252/embr.201846783.
26. Augello MA, Liu DL, Deonarine LD, Robinson BD, Huang D, Stelloo S, et al. CHD1 Loss Alters AR Binding at Lineage-Specific Enhancers and Modulates Distinct Transcriptional Programs to Drive Prostate Tumorigenesis (vol 35, pg 603, 2019). Cancer Cell 2019;35(5):817–9 doi 10.1016/j.ccell.2019.04.012. [PubMed: 31085180]
27. Zhang Z, Zhou C, Li X, Barnes SD, Deng S, Hoover E, et al. Loss of CHD1 Promotes Heterogeneous Mechanisms of Resistance to AR-Targeted Therapy via Chromatin Dysregulation. Cancer Cell 2020;37(4):584–98 e11 doi 10.1016/j.ccell.2020.03.001. [PubMed: 32220301]
28. Zhao D, Lu X, Wang G, Lan Z, Liao W, Li J, et al. Synthetic essentiality of chromatin remodelling factor CHD1 in PTEN-deficient cancer. Nature 2017;542(7642):484–8 doi 10.1038/nature21357. [PubMed: 28166537]
29. Zhao D, Cai L, Lu X, Liang X, Li J, Chen P, et al. Chromatin Regulator, CHD1, Remodels the Immunosuppressive Tumor Microenvironment in PTEN-Deficient Prostate Cancer. Cancer Discov 2020 doi 10.1158/2159-8290.CD-19-1352.
30. Yang W, Soares J, Greninger P, Edelman EJ, Lightfoot H, Forbes S, et al. Genomics of Drug Sensitivity in Cancer (GDSC): a resource for therapeutic biomarker discovery in cancer

cells. Nucleic Acids Res 2013;41(Database issue):D955–61 doi 10.1093/nar/gks1111. [PubMed: 23180760]

31. Garnett MJ, Edelman EJ, Heidorn SJ, Greenman CD, Dastur A, Lau KW, et al. Systematic identification of genomic markers of drug sensitivity in cancer cells. Nature 2012;483(7391):570–5 doi 10.1038/nature11005. [PubMed: 22460902]
32. Barretina J, Caponigro G, Stransky N, Venkatesan K, Margolin AA, Kim S, et al. The Cancer Cell Line Encyclopedia enables predictive modelling of anticancer drug sensitivity. Nature 2012;483(7391):603–7 doi 10.1038/nature11003. [PubMed: 22460905]
33. Kim D, Pertea G, Trapnell C, Pimentel H, Kelley R, Salzberg SL. TopHat2: accurate alignment of transcriptomes in the presence of insertions, deletions and gene fusions. Genome Biol 2013;14(4):R36 doi 10.1186/gb-2013-14-4-r36. [PubMed: 23618408]
34. Frankish A, Diekhans M, Ferreira AM, Johnson R, Jungreis I, Loveland J, et al. GENCODE reference annotation for the human and mouse genomes. Nucleic Acids Res 2019;47(D1):D766–D73 doi 10.1093/nar/gky955. [PubMed: 30357393]
35. Anders S, Pyl PT, Huber W. HTSeq--a Python framework to work with high-throughput sequencing data. Bioinformatics 2015;31(2):166–9 doi 10.1093/bioinformatics/btu638. [PubMed: 25260700]
36. Anders S, Huber W. Differential expression analysis for sequence count data. Genome Biol 2010;11(10):R106 doi 10.1186/gb-2010-11-10-r106. [PubMed: 20979621]
37. Beltran H, Prandi D, Mosquera JM, Benelli M, Puca L, Cyrta J, et al. Divergent clonal evolution of castration-resistant neuroendocrine prostate cancer. Nat Med 2016;22(3):298–305 doi 10.1038/nm.4045. [PubMed: 26855148]
38. Beltran H, Eng K, Mosquera JM, Sigaras A, Romanel A, Rennert H, et al. Whole-Exome Sequencing of Metastatic Cancer and Biomarkers of Treatment Response. JAMA Oncol 2015;1(4):466–74 doi 10.1001/jamaoncol.2015.1313. [PubMed: 26181256]
39. Niu H, Manfredi M, Ecsedy JA. Scientific Rationale Supporting the Clinical Development Strategy for the Investigational Aurora A Kinase Inhibitor Alisertib in Cancer. Front Oncol 2015;5:189 doi 10.3389/fonc.2015.00189. [PubMed: 26380220]
40. Eyers PA, Erikson E, Chen LG, Maller JL. A novel mechanism for activation of the protein kinase Aurora A. Curr Biol 2003;13(8):691–7 doi 10.1016/s0960-9822(03)00166-0. [PubMed: 12699628]
41. Dodson CA, Bayliss R. Activation of Aurora-A kinase by protein partner binding and phosphorylation are independent and synergistic. J Biol Chem 2012;287(2):1150–7 doi 10.1074/jbc.M111.312090. [PubMed: 22094468]
42. Zorba A, Buosi V, Kutter S, Kern N, Pontiggia F, Cho YJ, et al. Molecular mechanism of Aurora A kinase autophosphorylation and its allosteric activation by TPX2. Elife 2014;3 doi ARTN e0266710.7554/eLife.02667.
43. Bayliss R, Burgess SG, McIntyre PJ. Switching Aurora-A kinase on and off at an allosteric site. Febs J 2017;284(18):2947–54 doi 10.1111/febs.14069. [PubMed: 28342286]
44. Eyers PA, Churchill ME, Maller JL. The Aurora A and Aurora B protein kinases: a single amino acid difference controls intrinsic activity and activation by TPX2. Cell Cycle 2005;4(6):784–9 doi 10.4161/cc.4.6.1693. [PubMed: 15908779]
45. Lake EW, Muretta JM, Thompson AR, Rasmussen DM, Majumdar A, Faber EB, et al. Quantitative conformational profiling of kinase inhibitors reveals origins of selectivity for Aurora kinase activation states. Proc Natl Acad Sci U S A 2018;115(51):E11894–E903 doi 10.1073/pnas.1811158115. [PubMed: 30518564]
46. Bibby RA, Tang C, Faisal A, Drosopoulos K, Lubbe S, Houlston R, et al. A cancer-associated aurora A mutant is mislocalized and misregulated due to loss of interaction with TPX2. J Biol Chem 2009;284(48):33177–84 doi 10.1074/jbc.M109.032722. [PubMed: 19801554]
47. Schatz CA, Santarella R, Hoenger A, Karsenti E, Mattaj IW, Gruss OJ, et al. Importin alpha-regulated nucleation of microtubules by TPX2. Embo J 2003;22(9):2060–70 doi DOI 10.1093/emboj/cdg195. [PubMed: 12727873]

48. Safari MS, King MR, Brangwynne CP, Petry S. Interaction of spindle assembly factor TPX2 with importins-alpha/beta inhibits protein phase separation. J Biol Chem 2021;297(3):100998 doi 10.1016/j.jbc.2021.100998. [PubMed: 34302807]

49. Gruss OJ, Carazo-Salas RE, Schatz CA, Guarguaglini G, Kast J, Wilm M, et al. Ran induces spindle assembly by reversing the inhibitory effect of importin alpha on TPX2 activity. Cell 2001;104(1):83–93 doi 10.1016/s0092-8674(01)00193-3. [PubMed: 11163242]

50. Tsai MY, Wiese C, Cao K, Martin O, Donovan P, Ruderman J, et al. A Ran signalling pathway mediated by the mitotic kinase Aurora A in spindle assembly. Nat Cell Biol 2003;5(3):242–8 doi 10.1038/ncb936. [PubMed: 12577065]

51. Toya M, Terasawa M, Nagata K, Iida Y, Sugimoto A. A kinase-independent role for Aurora A in the assembly of mitotic spindle microtubules in Caenorhabditis elegans embryos. Nat Cell Biol 2011;13(6):708–14 doi 10.1038/ncb2242. [PubMed: 21572421]

52. Ding Z, Wu CJ, Chu GC, Xiao Y, Ho D, Zhang J, et al. SMAD4-dependent barrier constrains prostate cancer growth and metastatic progression. Nature 2011;470(7333):269–73 doi 10.1038/nature09677. [PubMed: 21289624]

53. Puca L, Bareja R, Prandi D, Shaw R, Benelli M, Karthaus WR, et al. Patient derived organoids to model rare prostate cancer phenotypes. Nat Commun 2018;9(1):2404 doi 10.1038/s41467-018-04495-z. [PubMed: 29921838]

54. Owonikoko TK, Niu H, Nackaerts K, Csoszi T, Ostoros G, Mark Z, et al. Randomized Phase II Study of Paclitaxel plus Alisertib versus Paclitaxel plus Placebo as Second-Line Therapy for SCLC: Primary and Correlative Biomarker Analyses. J Thorac Oncol 2020;15(2):274–87 doi 10.1016/j.jtho.2019.10.013. [PubMed: 31655296]

55. Cancer Genome Atlas Research N. The Molecular Taxonomy of Primary Prostate Cancer. Cell 2015;163(4):1011–25 doi 10.1016/j.cell.2015.10.025. [PubMed: 26544944]

56. Aparicio AM, Shen L, Tapia EL, Lu JF, Chen HC, Zhang J, et al. Combined Tumor Suppressor Defects Characterize Clinically Defined Aggressive Variant Prostate Cancers. Clin Cancer Res 2016;22(6):1520–30 doi 10.1158/1078-0432.CCR-15-1259. [PubMed: 26546618]

57. Asteriti IA, Daidone F, Colotti G, Rinaldo S, Lavia P, Guarguaglini G, et al. Identification of small molecule inhibitors of the Aurora-A/TPX2 complex. Oncotarget 2017;8(19):32117–33 doi 10.18632/oncotarget.16738. [PubMed: 28389630]

58. Adhikari B, Bozilovic J, Diebold M, Schwarz JD, Hofstetter J, Schroder M, et al. PROTAC-mediated degradation reveals a non-catalytic function of AURORA-A kinase. Nat Chem Biol 2020;16(11):1179–88 doi 10.1038/s41589-020-00652-y. [PubMed: 32989298]

Significance

CHD1 plays a critical role in controlling AURKA activation and promoting Aurora kinase inhibitor sensitivity, providing a potential clinical biomarker to guide cancer treatment.

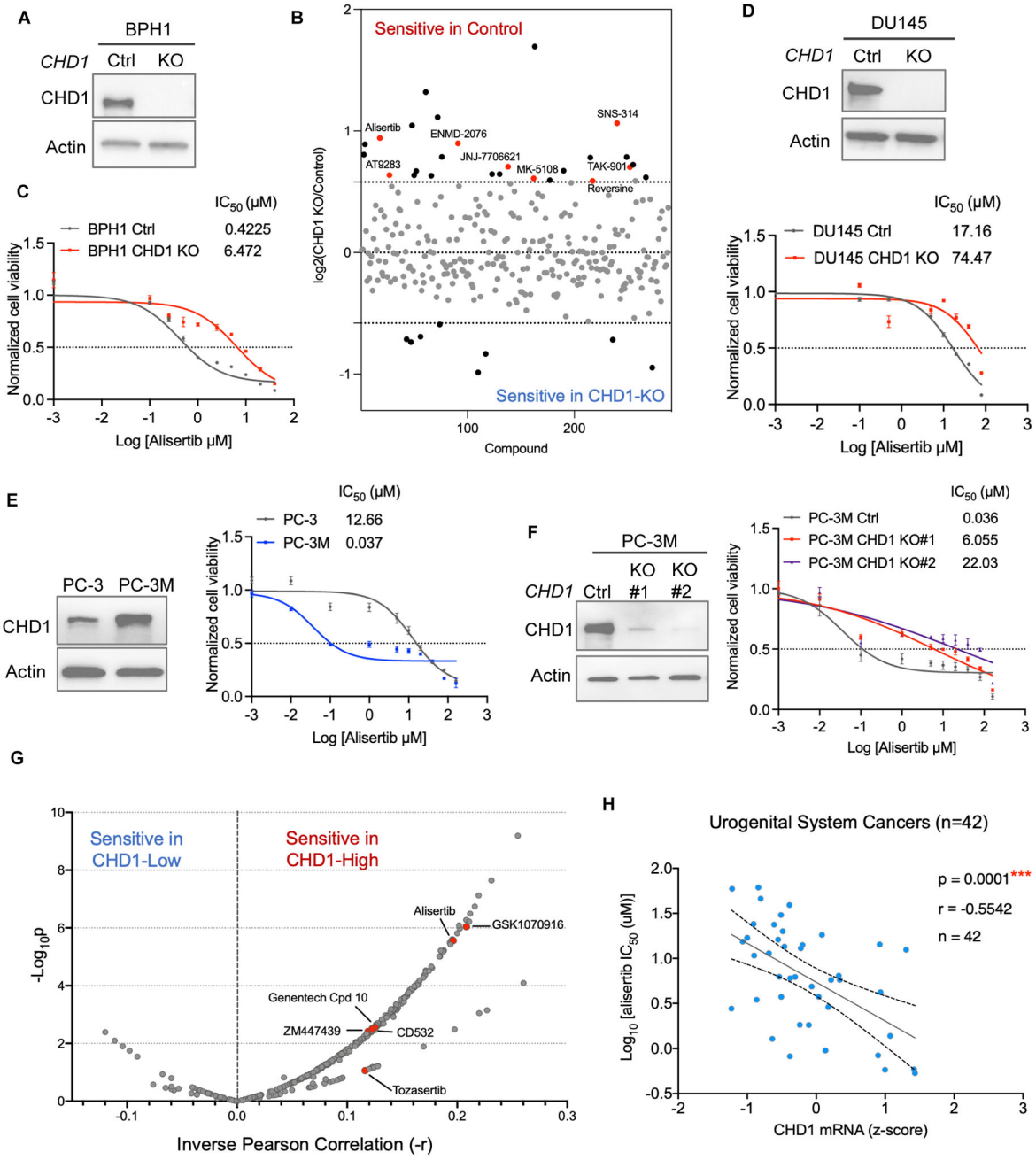

Figure 1. CHD1 renders cancer cells vulnerable to inhibitors targeting Aurora A.

A, Western blot of CHD1 in control and *CHD1* KO BPH1 cells. **B**, Differential responses of control and CHD1 KO cells to 287 compounds in initial epigenetic screen. Fold change of CHD1 KO cell viability versus control cell viability after treatment of individual compound (10uM, 72h) was presented. Thresholds of log2 (fold change) are 0.58 and −0.58. Aurora A inhibitors with differential responses in control and CHD1 KO cells were highlighted in red. **C-F**, Western blot of CHD1, dose-response curves, and IC_{50} values (μM) of alisertib in control and *CHD1* KO BPH1 (**C**) and DU145 cells (**D**), PC-3 and PC-3M cells (**E-F**). Cells were treated with the indicated concentrations of alisertib for 72 h. Data represent the

mean ± standard deviation of triplicates. IC_{50} values (μM) was calculated using GraphPad Prism version 9.2.0. **G**, Pan-cancer correlation analyses of CHD1 mRNA expression and drug sensitivity of 367 compounds. Inverse Pearson correlation coefficient (-r) and p values of all 367 compounds were presented in a volcano plot. Inhibitors targeting Aurora A are highlighted in red. **H**, Correlation between CHD1 expression and alisertib IC_{50} values (μM) in urogenital system cancer cell lines. Pearson correlation coefficient (r) and p values are shown. ***p<0.001.

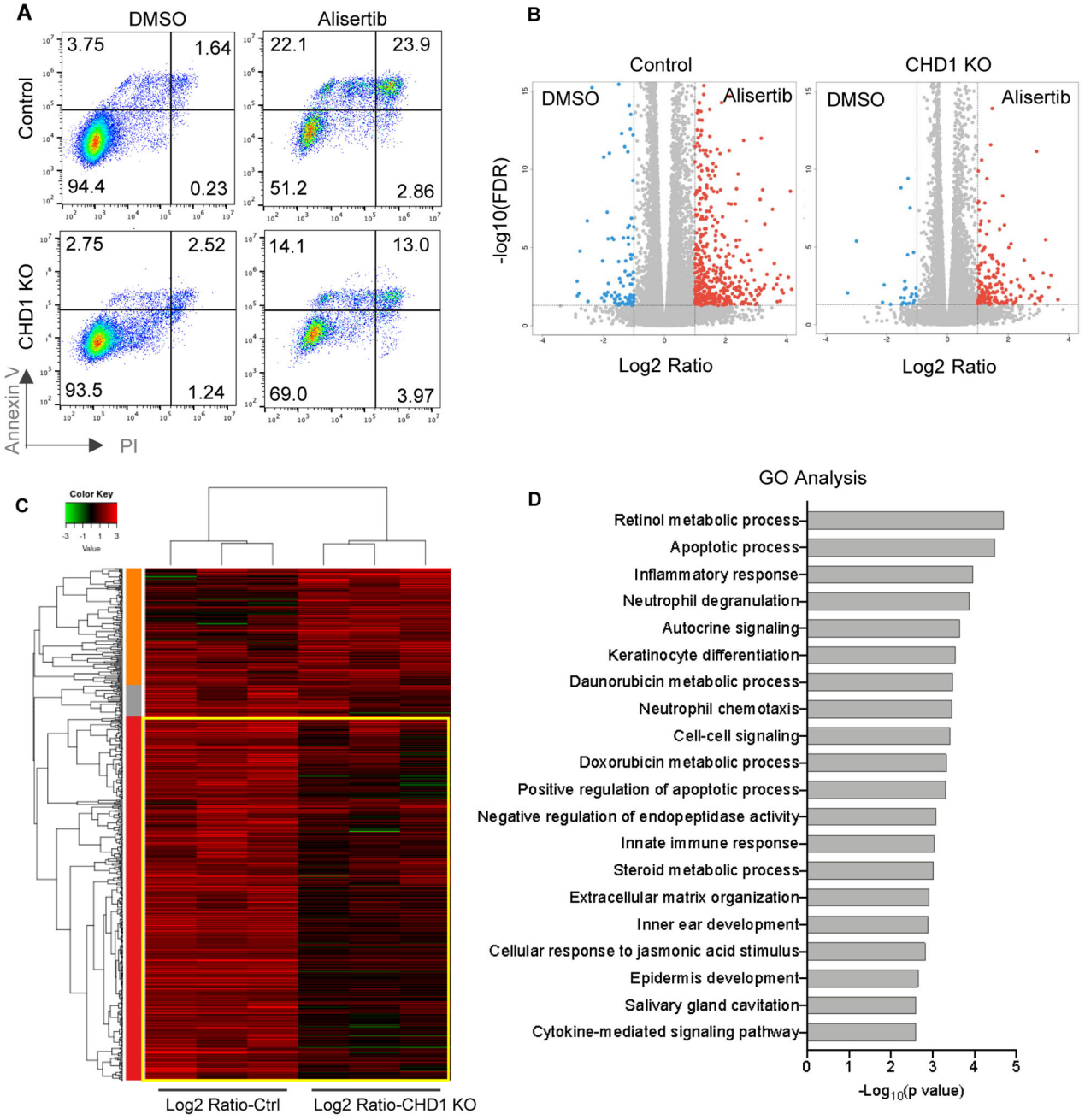

Figure 2. CHD1 is required for the apoptotic process induced by Aurora A inhibitor.

A, Flow cytometric analysis of control and CHD1 KO BPH1 cells stained with Annexin V and propidium iodide (PI), cells were treated with 1 μM alisertib for 48 h. The percentage of early (Annexin V+/PI−) and late apoptotic cells (Annexin V+/PI+) are shown. **B**, Volcano plots of differentially expressed genes (DEGs) in control and CHD1 KO BPH1 cells upon alisertib treatment. Up- and down-regulated genes after treatment are presented as red and blue dots, respectively. Thresholds of false discovery rate (FDR, 0.05) and fold change (FC, 2) are presented. **C**, Heatmap of 618 DEGs that were upregulated in alisertib-treated control or CHD1 KO cells (FDR≤0.05 and FC≥2) using log2 ratio values. Red and green

indicate upregulation and downregulation of gene expression, respectively. Yellow rectangle highlighted DEGs that were uniquely elevated in control cells in the presence of alisertib. **D**, Gene Ontology analysis of 439 DEGs that were uniquely elevated in alisertib-treated control cells. Top 20 biological processes are presented and ranked by p value.

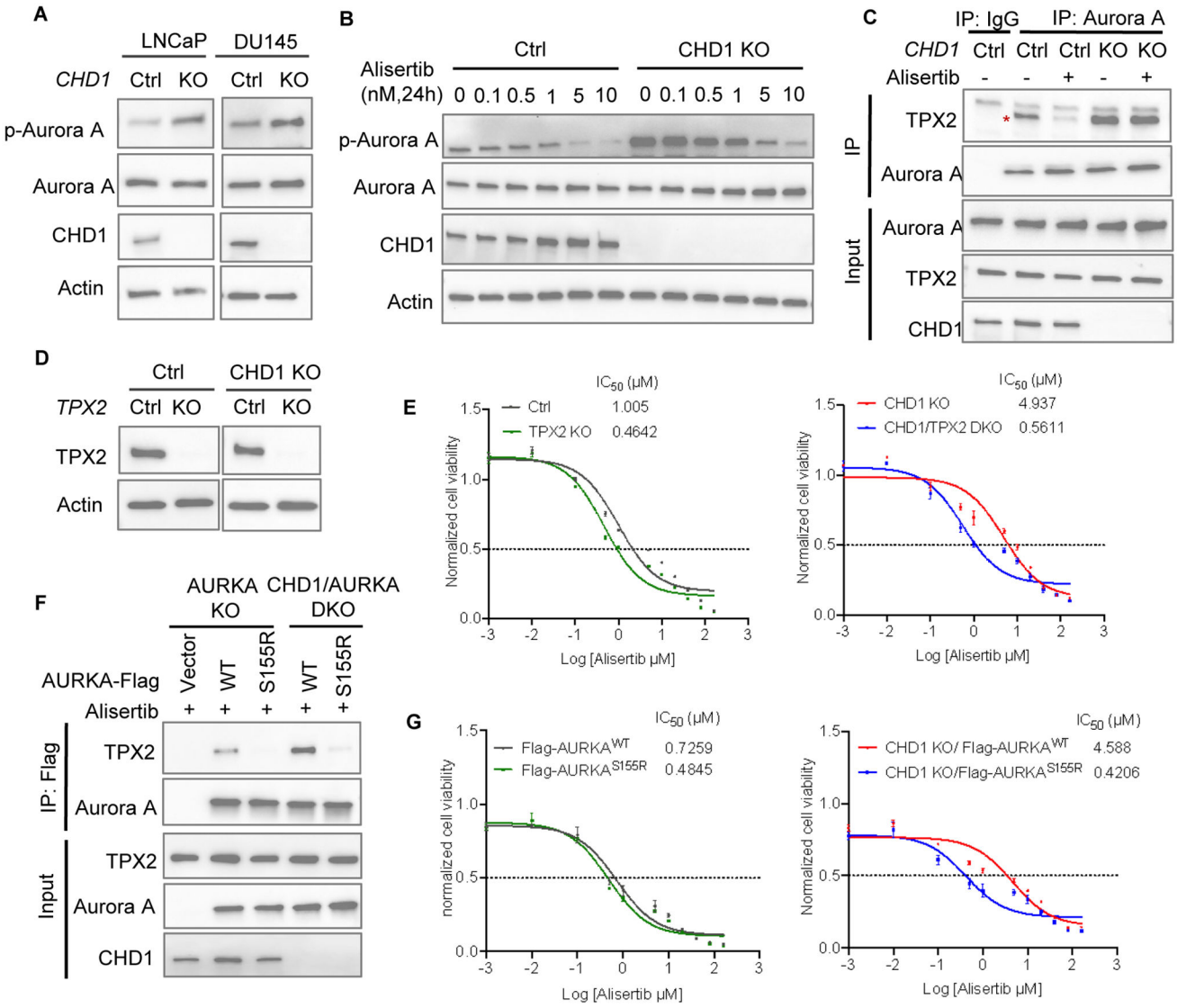

Figure 3. CHD1 controls Aurora A by modulating its interaction with TPX2.

A, Western blot analysis of Aurora A and phospho-Aurora A (Thr288) in control and CHD1 KO prostate cancer cell lines. **B**, Western blot analysis of Aurora A and phospho-Aurora A (Thr288) in control and CHD1 KO DU145 cell lines treated with the indicated concentrations of alisertib for 24 h. **C**, Endogenous coimmunoprecipitation (co-IP) of TPX2 and Aurora A in control and CHD1 KO BPH1 cells treated with or without alisertib (10 μM, 24h). The asterisk indicates TPX2 protein. **D-E**, Western blot analysis of TPX2 (**D**) and IC_{50} values (μM) of alisertib (**E**) in control and CHD1 KO BPH1 cells with or without TPX2 KO. Cells were treated with the indicated concentrations of Alisertib for 72 h. **F-G**, AURKA KO and CHD1/AURKA DKO BPH1 cell lines were constructed, followed by transduction of Flag-tagged WT or S155R-mutated AURKA. Cells were treated with 10 μM alisertib for 24 h, followed by co-IP to assess the interaction of TPX2 and Aurora A (**F**). Cells were treated with the indicated concentrations of alisertib for 72 h to assess IC_{50} values (μM) (**G**). Cell

viability was quantified by luminescence. Data represent the mean ± standard deviation of triplicates. IC_{50} was calculated using GraphPad Prism version 9.2.0.

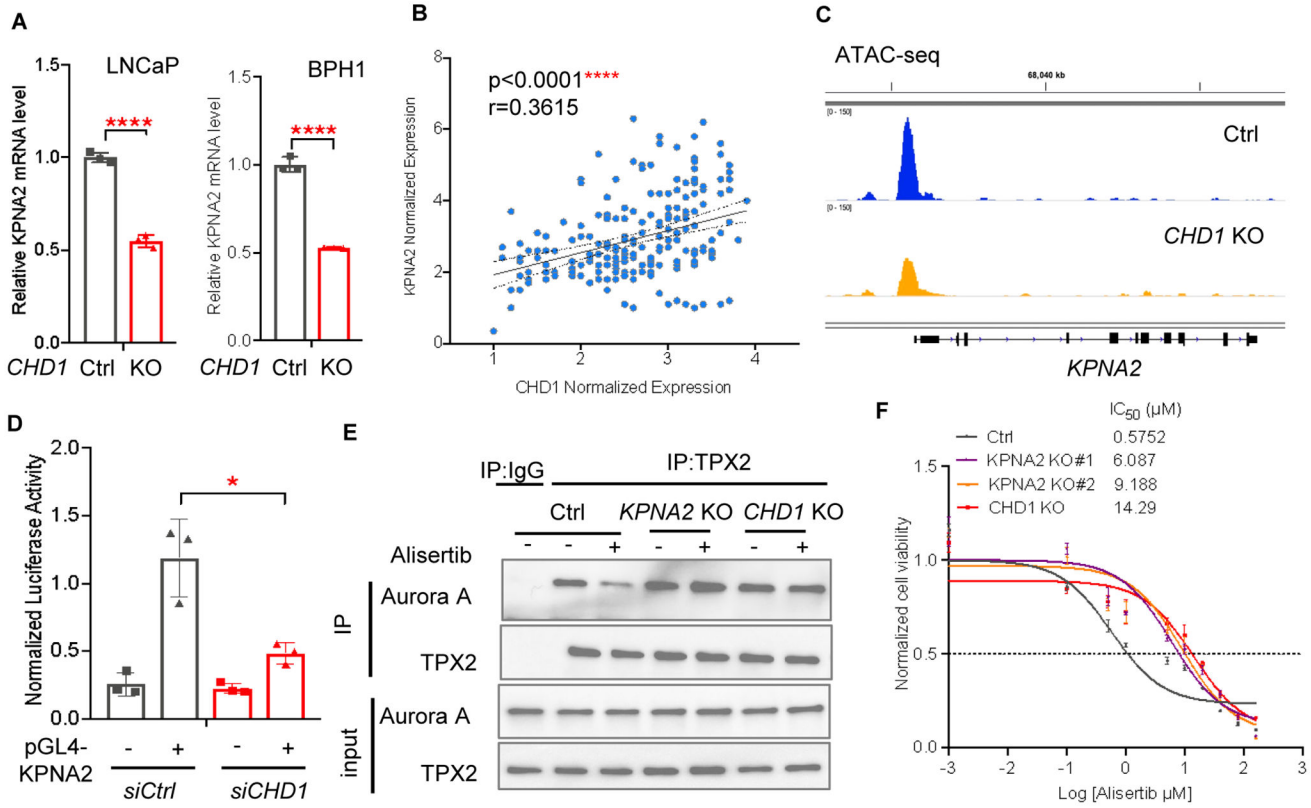

Figure 4. The axis of CHD1-KPNA2 controls the interaction of TPX2 and Aurora A.

A, Expression of *KPNA2* gene in control and CHD1 KO LNCaP and BPH1 cells. Data represent the mean ± standard deviation of triplicates. An unpaired two-tailed Student's t-test was used for statistical analysis. ****p<0.0001. **B**, Pearson correlation analysis shows positive correlation between CHD1 and KPNA2 in human prostate cancer samples. Pearson correlation coefficient (r), and p values are shown, ****p<0.0001. **C**, ATAC-seq analysis of promoter accessibility of *KPNA2* gene in control and CHD1 KO LNCaP cells. **D**, Dual luciferase assay was conducted to detect the transcriptional activation of *KPNA2* gene. Renilla luciferase plasmid and control or pGL4 plasmid containing a 1.2-kb DNA fragment of *KPNA2* promoter were transfected into LNCaP cells with or without CHD1 knockdown, followed by a dual luciferase assay. Data represent the mean ± standard deviation of triplicates. An unpaired two-tailed Student's t-test was used for statistical analysis. *$p < 0.05$. **E**, Endogenous co-IP of TPX2 and Aurora A in control, KPNA2 KO, and CHD1 KO BPH1 cells treated with or without 10 μM alisertib for 24 h. **F**, IC_{50} values (μM) of alisertib in control, KPNA2 KO and CHD1 KO BPH1 cell lines. Cells were treated with the indicated concentrations of alisertib for 72 h. Cell viability was quantified by luminescence. Data represent the mean ± standard deviation of triplicates. IC_{50} was calculated using GraphPad Prism version 9.2.0.

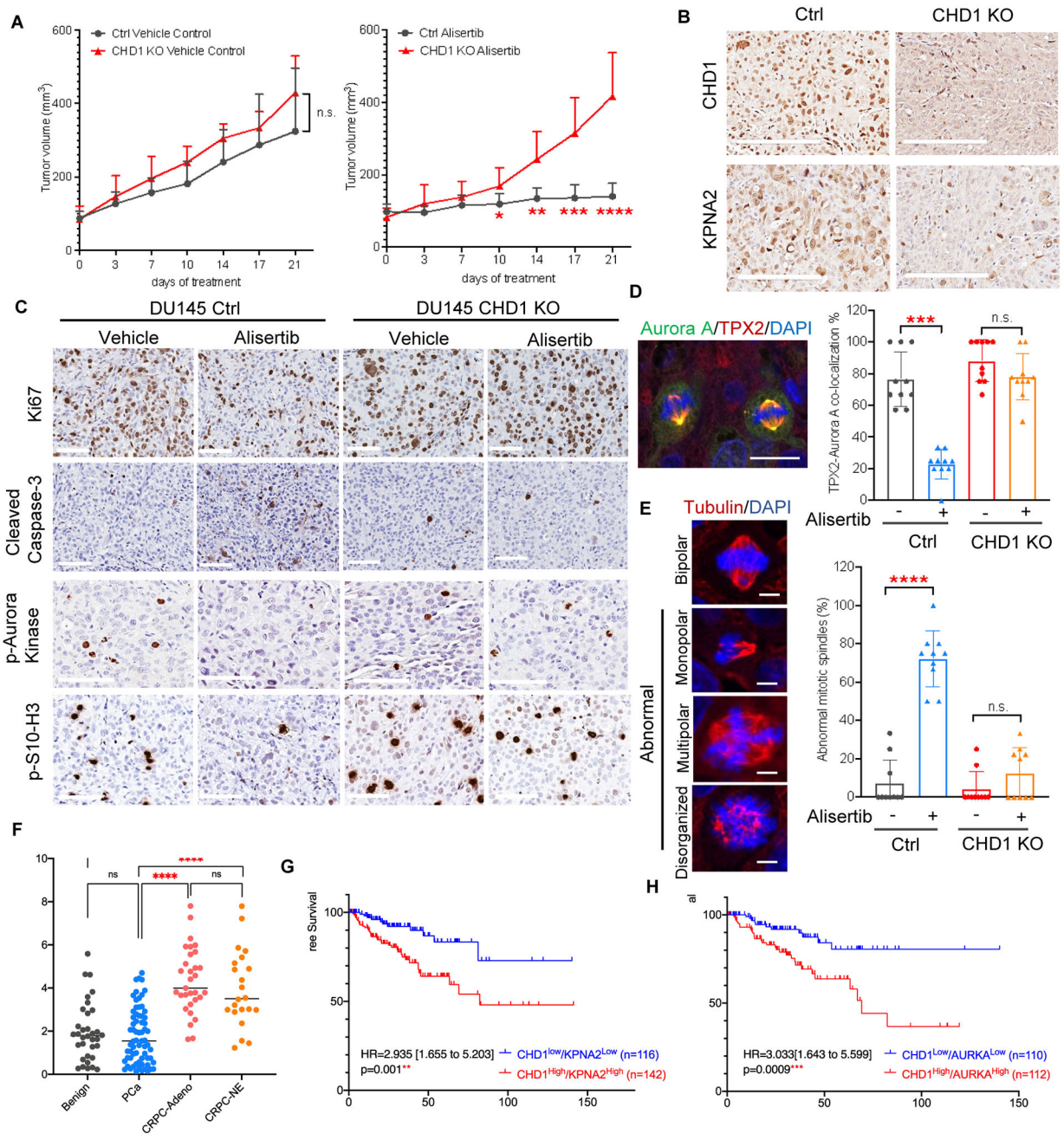

Figure 5. CHD1 is required for the anti-tumor effects of alisertib in vivo.

A, Xenograft prostate cancer mouse models were established using control and CHD1 KO DU145 cells. Mice were treated with vehicle or alisertib (10 mg/kg/day) by oral gavage daily for 21 days. Tumor size was measured twice a week. n=6–8 mice. An unpaired two-tailed Student's t-test was used for statistical analysis. *p < 0.05; **p < 0.01; ***p < 0.001; ****p < 0.0001; n.s.: not significant. **B**, Representative images of immunohistochemistry (IHC) staining for CHD1 and KPNA2 in xenograft tumors derived from control and CHD1 KO DU145 cells. Scale bar=200 μm. **C**, Representative images of IHC staining for Ki67, Cleaved caspase-3, phospho-Aurora Kinase, and phospho-Histone

H3 (Ser10) in control and CHD1 KO DU145 derived xenograft tumors after treatment. Scale bar=100 μm. **D**, Immunofluorescence (IF) co-staining of TPX2 (red) and Aurora A (green) in control and CHD1 KO DU145 derived xenograft tumors after treatment. Representative image of TPX2-Aurora A co-localization is presented (Scale bar=20 μm). Quantification shows the percentage of mitotic cells with TPX2-Aurora A co-localization in each group. **E**, Spindle assembly (red: tubulin) and chromosome alignment (blue: DAPI) in control and CHD1 KO DU145 derived xenograft tumors after treatment. Representative images of abnormal mitotic spindles are presented (Scale bar=5 μm). Quantification shows the percentage of mitotic cells with abnormal mitotic spindles. Data represent the mean ± standard deviation of 10 individual views. An unpaired two-tailed Student's t-test was used for statistical analysis. ***p<0.001; ****p<0.0001. n.s.: not significant. **F**, Expression of CHD1 in different stage of human prostate cancer determined by RNA-seq (n=155). ****p<0.0001. n.s.: not significant. **G-H**, Clinical relevance of CHD1/KPNA2 (**G**) and CHD1/AURKA (**H**) expression with progression-free survival in human prostate cancer. Log-rank (Mantel-Cox) test was used for statistical analysis. *p < 0.05. HR [95% confidence interval (CI)] are presented.

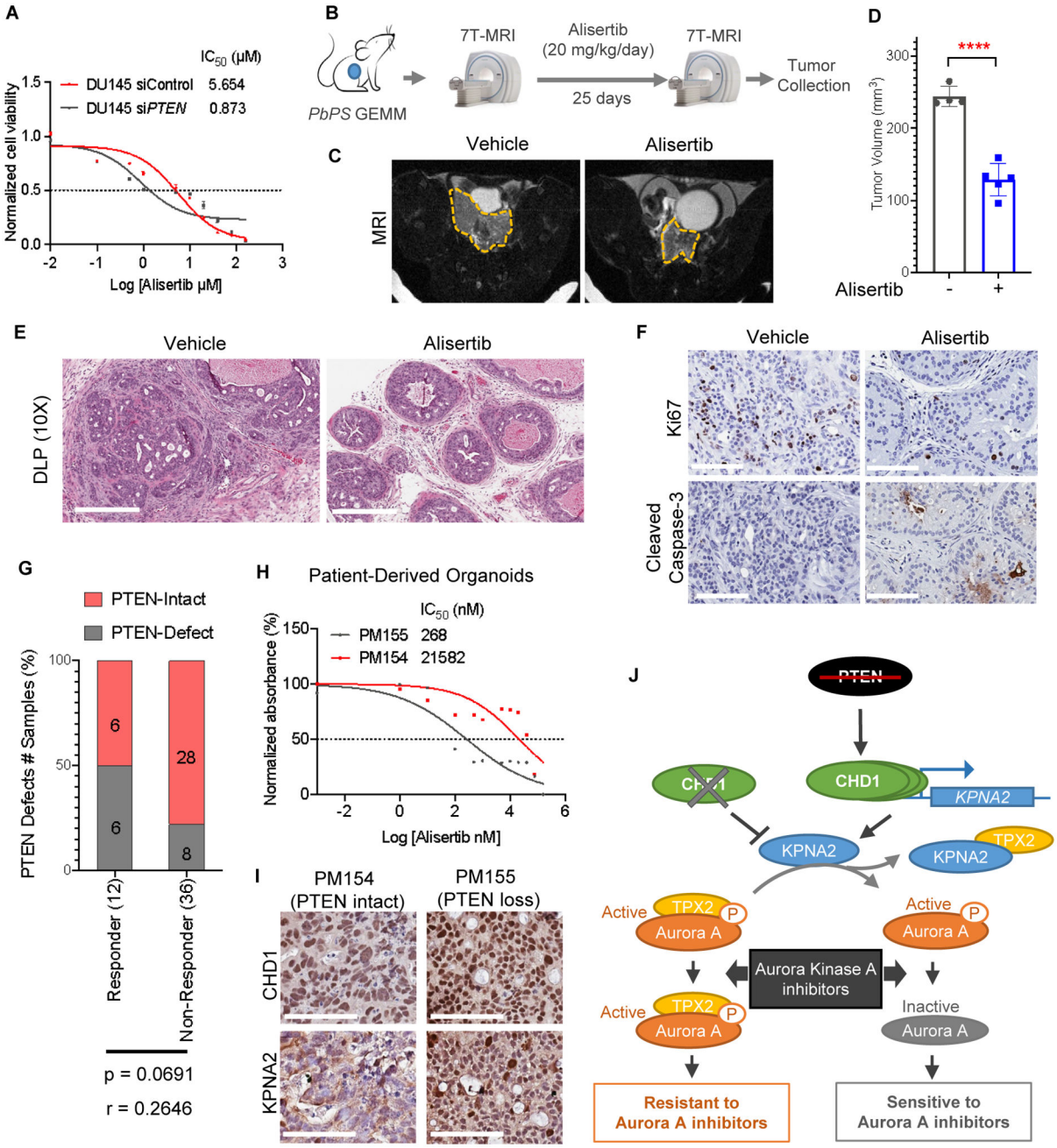

Figure 6. PTEN defects are associated with a better response to alisertib in advanced prostate cancer.

A, IC_{50} values (μM) of alisertib in DU145 cells transfected with control and PTEN siRNA. Cells were treated with the indicated concentrations of alisertib for 72 h. Data represent the mean ± standard deviation of triplicates. IC_{50} was calculated using GraphPad Prism version 9.2.0. **B**, Schematic of drug treatment design using genetically engineered mouse models (GEMMs) *PB-Cre; PtenL/L; Smad4L/L (PbPS)*. Tumor volume was monitored by 7T-MRI. **C-D**, Representative MRI scan(**C**) and tumor volume (**D**) of prostate tumors from PbPS mice after 25-day treatment of vehicle control or alisertib (20 mg/kg/day) by oral gavage

daily. n=4–5 mice. Data represent the mean ± standard deviation. Statistical analyses were performed using an unpaired two-tailed Student t-test with GraphPad Prism version 9.2.0. ****p<0.0001. **E**, Representative H&E staining of dorsal-lateral prostate (DLP) tumors at the endpoint. Scale bar=300 μm**. F** Representative images of IHC staining of Ki67 and Cleaved caspase-3 in DLP tumors. Scale bar=100 μm. **G**, Percentage of patients with PTEN defects in responder or non-responder groups in phase II clinical trial of alisertib in mCRPC. Pearson correlation analysis was performed using GraphPad Prism version 9.2.0.. **H**, Patient-derived organoids PM155 (PTEN-loss) and PM154 (PTEN-intact) were treated with the indicated concentrations of alisertib for 6 days to assess IC_{50} values (nM). Cell viability was quantified by luminescence. Data represent the mean ± standard deviation of 5 replicates. IC_{50} was calculated using GraphPad Prism version 9.2.0. **I**, Representative images of IHC staining of CHD1 and KPNA2 in PM155 and PM154 organoids. Scale bar=100 μm. **J**, Schematic model.